Theoret. Comput. Fluid Dynamics (1999) 13: 77–90

Theoretical and Computational Fluid Dynamics

Temporal Stability of Boundary-Free Shear Flows: The Effects of Diffusion

A. Öztekin, L.J. Cumbo, and A. Liakopoulos

Department of Mechanical Engineering and Mechanics, Lehigh University, Bethlehem, PA 18105, U.S.A.

Communicated by M.Y. Hussaini

Received 8 January 1998 and accepted 4 February 1999

Abstract. The stability of boundary-free shear flow is studied for the case of variable viscosity due to binary diffusion across the shear layer. This leads to the main difficulty of this investigation, the direct coupling of the momentum and species equations in both the base state calculations as well as the stability analysis.

Linear stability analysis is used to examine the effect of a nonuniform concentration profile on the stability of the flow. It is found that for the flow to be stable for all disturbance wave numbers the Reynolds number has to be zero. This is in agreement with constant viscosity free shear flow stability theory. Increasing the magnitude of concentration gradient (increasing the Schmidt number) destabilizes the flow.

1. Introduction

The problem of predicting the stability characteristics of free shear flows is of great theoretical and practical importance. These flows occur in systems of various scales. Large-scale examples are found in natural processes in the atmosphere and the oceans. These geophysical flows include flows in stratified estuaries as well as high shear regions in oceanic thermoclines and temperature inversions in the atmosphere. Medium- and small-scale examples are those found in engineering systems, especially in environmental, aeronautical, and industrial engineering applications. Such examples include wastewater discharges into bays, artificial destratification in reservoirs, reacting free shear layer flows in combustors and rockets, flow of a polymeric fluid or fluids-in-layer in polymer processing systems, and flows in dendritic- and plane-front solidification of binary or multicomponent systems. In many of these systems, concentration gradients and diffusion of species can play an important role in the structure and stability of boundary-free shear flows. In some of these systems, fluid viscosity can be strongly dependent on the concentration. For example: the viscosity of polymeric solutions and melts is sensitively dependent on concentration (Bird *et al.*, 1987a, b), and the viscosity of a mixture of gases can be a strong function of mole fractions (Maitland *et al.*, 1981). This work focuses on the hydrodynamic aspects of isothermal free shear flows in which mass diffusion is present. It is vital to understand the mechanisms that control the stability characteristics of these flows. In the context of engineering systems this understanding allows for the design of processes that may either passively depend on flow stability or may actively govern the development of the flow.

Boundary-free flows, such as mixing layers, wakes, and jets, are highly unstable when compared with bounded flows. This is attributed to the presence of an inflection point in the velocity profile and the associated inviscid instability. Boundary-free flows are characterized by lower values of the critical Reynolds number at the onset of hydrodynamic instability (the highest Reynolds number for which the flow is stable for all

wave numbers of a disturbance) and a larger range of wave numbers for which these flows are unstable when compared with flows that do not have a velocity profile inflection. Specifically, the constant-property incompressible free shear layer has a critical Reynolds number of zero, i.e., the flow is not stable for all wave numbers at any finite value of Reynolds number, R.

Early studies of linear stability of mixing layers in incompressible parallel inviscid flows were performed by Helmholtz (1868) and Kelvin (1871). The instability mode they discovered, referred to as Kelvin–Helmholtz instability, involves a growing wavy disturbance across the surface of discontinuity in the initial velocity field. Rayleigh developed his point-of-inflection theorem from the study of incompressible parallel inviscid flows with continuous velocity profiles. Rayleigh's theorem states that a necessary (but not sufficient) condition for instability of inviscid flow is that the basic state velocity profile has an inflection point. Fjørtoft's theorem (Panton, 1984) improves on Rayleigh's statement by being more selective. It shows that not all profiles with an inflection point satisfy the necessary condition for instability. It was shown by Tollmien that an inflection point is not only necessary but, in certain circumstances, a sufficient condition for instability, as well.

The first stability investigation of a realistic free, boundary-layer type, parallel shear flow was reported by Lessen (1950). Lessen's power-series-expansion method of solving the stability equations allowed for only studying the large Reynolds number limit. Therefore, he did not identify a Reynolds number for which the flow was completely stable. Esch (1957) reported a critical Reynolds number of zero for a boundary-free flow with a piecewise linear velocity profile. Tatsumi and Gotoh (1959) studied the stability of boundary-free flows with a velocity profile of general form and reported that the critical Reynolds numbers for these flows was zero.

Drazin and Howard (1962) studied the instability characteristics of the hyperbolic-tangent profile for small wave-number disturbances. Later Michalke (1964) obtained the eigenvalues and eigenfunctions of the inviscid Rayleigh equation for the same profile. Betchov and Szewczyk (1963) examined the stability of a Newtonian viscous flow with hyperbolic-tangent profile by solving the Orr–Sommerfeld equation and concluded that the flow is not stable for all wave numbers for any value of Reynolds number, i.e., the critical Reynolds number is zero. A review of the linear stability theory is given in Betchov and Criminale (1967) and Drazin and Reid (1981). A comprehensive review of the stability and the structure of the free shear flows is given in Ho and Huerre (1984).

Compressibility and viscoelastic aspects of the mixing layer problem have also been investigated. Azaiez and Homsy (1993) used linear stability analyses and direct numerical simulations to study the elastic effects on the stability of two-dimensional incompressible mixing layers of viscoelastic fluids. Jackson and Grosch (1989, 1990a, b, 1991) and Grosch and Jackson (1991) have studied the stability of unconfined compressible nonreacting and reacting mixing layers. They performed inviscid spatial stability analysis to study various aspects of the compressible mixing layers. Shin and Ferziger (1993) have studied the stability of the confined compressible reacting mixing layer.

Jackson and Grosch (1990b) have conducted a stability calculation of a compressible mixing layer of a gas mixture and have shown that the stability characteristics of the flow are dependent on the composition of the gas mixture. Kennedy and Gatski (1994) performed a theoretical analysis of the structure of supersonic mixing layers in binary gas mixtures. Their analysis included the variation of fluid density with the composition varying across the mixing layer. Jackson and Grosch (1994) have investigated the structure and stability of a laminar diffusion flame in a compressible, three-dimensional mixing layer. These investigators considered a three-dimensional, finite rate, reacting compressible mixing layer lying between two streams of reactants with different freestream speed and temperature. The fluid viscosity is considered to be a function of temperature. They employed numerical simulations and asymptotic analyses to study the flow structure and the stability of the system for different flow regimes. More recently, Kozusko *et al.* (1996a) have studied the structure of compressible mixing layers in binary gas mixtures, in which both heat and mass diffusion are present. They concluded that an accurate representation of the flow, temperature, and concentration fields could only be obtained by considering variations in the thermal properties with composition and temperature. The viscosity of the mixture was determined as a function of the mole fractions of the gases, the viscosity of the individual gases, and of the interaction viscosity arising from collisions between the molecules of the different gases. The viscosity of the individual gases as a function of temperature was calculated using the first-order kinetic theory given by Maitland *et al.* (1981). Kozusko *et al.* (1996b) have investigated the stability of parallel compressible mixing layers in binary gas mixtures by considering variations in the ther-

mophysical properties of the gas mixture with temperature and composition. They showed that molecular weights of the gases have a significant effect on the maximum growth rate, the phase speeds of the neutral and the unstable modes, and the frequency of the most-unstable disturbances.

The nonparallel effects on the stability of boundary layer, mixing, and free shear flows have been studied by several investigators. A number of investigators (Liu, 1974; Morris, 1971) have accomplished this using integral formulations involving an equation for amplitude variation in the streamwise direction. The spatial stability analysis of slowly diverging flows has been considered by Crighton and Gaster (1976) and Gaster *et al.* (1985) to study large-scale structures in jet and mixing layer flows by employing a slowly varying type of approximation or WKB method or a multiple scales arguments. Using a similar approach, Asrar and Nayfeh (1985) and Nayfeh and El-Hady (1980) have studied the nonparallel effects in boundary-layer flows when heat diffusion is present. They considered perturbations to the flow properties and to the physical properties of the fluid (density, viscosity, thermal diffusivity, and specific heat capacity are treated as functions of temperature). These authors studied the stability of both self-similar and nonsimilar base flow over a nonuniformly heated flat plate. They concluded that nonparallel effects hardly modify the stability characteristics of this flow but relaxing the self-similar assumption significantly alters the critical conditions and spatiotemporal nature of the secondary flow. Their results agree qualitatively with the experimental measurements of Strazisar and Reshotko (1978) when nonsimilar flow profiles are considered.

Stability calculations of two- and three-dimensional mixing layer flows have been reported. Corcos and Lin (1984) considered the three-dimensional instabilities of an evolving two-dimensional base flow. More recent studies of free shear flows investigate the transition to turbulence by considering large Reynolds numbers or nonlinear instability mechanisms. Metcalfe *et al.* (1987) examined the effects of the interaction between linear and nonlinear flow states on stability in the transitional regime by considering three-dimensional perturbations to two-dimensional base flow. Rogers and Moser (1992) studied the temporal development of a three-dimensional mixing layer through direct numerical simulations based on the three-dimensional unsteady Navier–Stokes equations. Sullivan and List (1994) examined the mixing and transport of a stratifying scalar at a density interface embedded in a turbulent shear flow.

In this paper we investigate the effect of viscosity variation with composition on the stability characteristics of an incompressible boundary-free shear flow. The combination of the species transport with the momentum transport phenomenon renders the fluid viscosity a function of the concentration level and leads to direct coupling of these two occurrences. Both the momentum (velocity) layer and concentration (mixing) layer equations are considered in the analysis. The basic flow equations as well as the stability equations are coupled.

The equations governing the free shear flow and the concentration field are described in Section 2. A similarity solution for the steady basic state velocity and concentration fields are presented together with equations governing the temporal stability of parallel boundary-free shear flows. The numerical techniques used to solve the basic state equations and the eigenvalue problem for the stability equations are also described in Section 2. The results are presented and discussed in Section 3 and conclusions are summarized in Section 4.

2. Formulation

In deriving the governing equations for the momentum transport and diffusion in the shear layer shown in Figure 1, we begin with the continuity, momentum, and species equations, assuming Newtonian fluid of constant density:

$$\nabla \cdot \boldsymbol{u} = 0 \tag{1a}$$

$$\rho \frac{\partial \boldsymbol{u}}{\partial t} + \rho(\boldsymbol{u} \cdot \nabla)\boldsymbol{u} = -\nabla p + \nabla \cdot (\mu \dot{\gamma}), \tag{1b}$$

$$\frac{\partial c}{\partial t} + \boldsymbol{u} \cdot \nabla c = \nabla \cdot (D \nabla c). \tag{1c}$$

Here $\boldsymbol{u}$ denotes the velocity vector, p is the pressure, μ denotes the absolute viscosity, $\dot{\gamma}$ is the rate-of-strain tensor, ρ is the density, D is the binary mass diffusion coefficient, and c is the concentration.

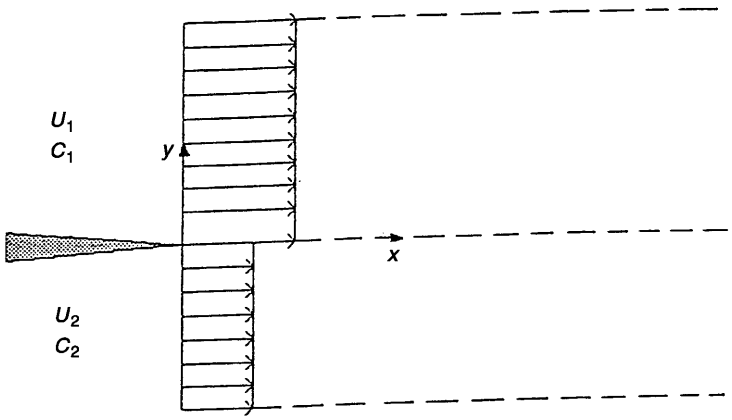

Figure 1. Flow schematic.

The far-field boundary conditions are

$$y \to +\infty, \qquad \boldsymbol{u} \to (U_1,\ 0,\ 0), \quad \text{and} \quad c \to C_1, \tag{2a}$$

$$y \to -\infty, \qquad \boldsymbol{u} \to (U_2,\ 0,\ 0), \quad \text{and} \quad c \to C_2, \tag{2b}$$

where U_1, U_2, C_1 and C_2 are the flow velocities and concentrations of the two initially separated fluid layers.

The viscosity of the fluid is approximated by

$$v = \frac{\mu}{\rho} = v_0(1 + ac^2), \tag{3}$$

where a is a positive number and v_0 is the kinematic viscosity at the reference state. This relation is derived by noting that v_{sp}/c versus c has a positive linear slope, where $v_{sp} = v/v_0 - 1$ (Shoemaker *et al.*, 1974).

2.1. Basic State Equations and Numerical Solution

In order to calculate the basic state steady velocity and concentration fields we implement standard boundary-layer analysis assuming that the basic state velocity in the x-direction is much greater than in the y-direction, and gradients of the basic state velocity and concentration normal to the x-direction are much larger than those parallel to it (Schlichting, 1979; Incropera and DeWitt, 1990). The governing equations for the steady basic state velocity and concentration fields are written as

$$\frac{\partial u_s}{\partial x} + \frac{\partial \mathrm{v_s}}{\partial y} = 0, \tag{4a}$$

$$u_s \frac{\partial u_s}{\partial x} + \mathrm{v_s} \frac{\partial u_s}{\partial y} = \frac{\partial}{\partial y}\left(v_s \frac{\partial u_s}{\partial y} \right), \tag{4b}$$

$$u_s \frac{\partial c_s}{\partial x} + \mathrm{v_s} \frac{\partial c_s}{\partial y} = D \frac{\partial^2 c_s}{\partial y^2}, \tag{4c}$$

where $(u_s,\ \mathrm{v_s})$ denote the streamwise and transverse components of the basic state velocity field, c_s is the basic state concentration field, and v_s is the fluid viscosity, defined by $v_s = v_0(1 + ac_s^2)$.

The velocity components are written in terms of a stream function, $\psi(x,\ y)$, i.e., $u_s \equiv \partial\psi/\partial y$ and $\mathrm{v_s} \equiv -\partial\psi/\partial x$. The continuity equation is now satisfied and no longer needed. We next define a similarity parameter $\eta(x,\ y) = y/\delta$. Noting that the boundary layer thickness δ is given by $\delta \propto (v_0 x/U_1)^{1/2}$, the similarity variable η can be written as

$$\eta \equiv y\sqrt{\frac{U_1}{v_0 x}} \tag{5}$$

while the stream function, velocity components, and concentration can now be written in terms of η:

$$\psi = f(\eta)\sqrt{\frac{v_0 x}{U_1}}, \qquad u_s = f', \qquad \mathrm{v_s} = \frac{1}{2}\sqrt{\frac{v_0}{U_1 x}}\,(\eta f' - f), \quad \text{and} \quad c_s = g(\eta). \tag{6}$$

Note that (u_s, $\mathrm{v_s}$) is now measured in units of U_1, c_s in units of C_1, and v_s in units of v_0. Substituting (6) into the momentum and species equations (4b,c) we obtain the following nonlinear differential equations for $f(\eta)$ and $g(\eta)$:

$$f''' + \frac{1}{\mathrm{v_s}} f''\left(\tfrac{1}{2} f + v_s'\right) = 0, \tag{7a}$$

$$g'' + \frac{Sc}{2} f g' = 0, \tag{7b}$$

where primes denote derivatives with respect to η and the Schmidt number, Sc, is defined as v_0/D. The boundary conditions for f and g are

$$\eta \to \infty, \qquad f' \to 1, \quad \text{and} \quad g \to 1, \tag{8a}$$

$$\eta \to -\infty, \qquad f' \to U^*, \quad \text{and} \quad g \to C^*, \tag{8b}$$

$$f(0) = 0, \tag{8c}$$

where $U^* = U_2/U_1$ and $C^* = C_2/C_1$. Boundary condition (8c) implies that at $y = 0$, where the initial mixing occurs, the stream function must be equal to zero since the motion is steady.

In order to discretize the problem, the domain ($-\infty < \eta < +\infty$) is truncated to ($-L \le \eta \le +L$). The base state velocity and concentration fields (f and g) are expanded in a series of Chebyshev polynomials. These expansions are simplified by transforming variable η of the computational domain ($-L \le \eta \le +L$) to $\xi = \eta/L$, so that the new variable satisfies ($-1 \le \xi \le +1$). The transformed set of ordinary differential equations are solved using the Galerkin technique developed by Zebib (1987), in which the highest derivative of the functions f and g are approximated by truncated sums of the form

$$f'''(\xi) = \sum_{i=0}^{N} b_{1i} T_i(\xi) \quad \text{and} \quad g''(\xi) = \sum_{i=0}^{N} b_{2i} T_i(\xi), \tag{9}$$

where T_i is the ith Chebyshev polynomial and the coefficients $\{b_{ji}\}$ for $j = \{1,\ 2\}$ are to be determined. Representations of the lower-order derivatives and the functions f and g are computed by integrating (9) and using standard properties of the Chebyshev polynomials.

The Galerkin procedure reduces the problem ((7) and (8)) to a nonlinear algebraic vector equation which is solved using the standard Newton's Acceleration of Convergence method. The details of this iterative method are discussed elsewhere by Öztekin *et al.* (1997). The iterative procedure is terminated when solutions obtained from two successive iterations differ less than one part in 10^{12}. Newton's method reduces the problem to a set of linear algebraic equations of the form

$$\boldsymbol{E}\boldsymbol{x} = \boldsymbol{F}, \tag{10}$$

where $\boldsymbol{x} = \delta[b_{1n},\ b_{2n},\ b_{3n},\ b_{4n},\ b_{5n}] \in \Re^{5(N+1)}$ is the perturbation vector of the coefficients. Elements of the coefficient matrices $\boldsymbol{E}$ and $\boldsymbol{F}$ are in the domain $\Re^{5(N+1)}$. The perturbation vector $\boldsymbol{x}$ at each iteration is computed using the algorithm coded in DLSLRG of the IMSL library.

2.2. Linear Disturbance Equations and Numerical Solution

Equations governing the linear stability of the base flow are formed by measuring length, velocity, concentration, pressure, and time in units of δ, U_1, C_1, ρU_1^2, δ/U_1, respectively. To determine the conditions under which a disturbance grows, we assume a quasi-two-dimensional flow (parallel flow) approximation ($\mathrm{v_s} = 0$), where the disturbances are analyzed at a fixed x location. Due to the fact that the base state velocity in the x-direction (u_s) and the concentration (c_s) are dependent on the functions $f(\eta)$ and $g(\eta)$, and x is fixed, these variables depend only on y for the disturbance equations. We also assume two-dimensional time-dependent

disturbances for the x and y velocity components as well as the concentration. The perturbed velocity, pressure, and concentration field is written as

$$\begin{bmatrix} \hat{u} \\ \hat{\mathrm{v}} \\ \hat{p} \\ \hat{c} \end{bmatrix}(x,y,t) = \begin{bmatrix} f' \\ 0 \\ p_s \\ g \end{bmatrix}(y) + \begin{bmatrix} u \\ \mathrm{v} \\ p \\ c \end{bmatrix}(x,y,t), \tag{11}$$

where $(\hat{u}, \hat{\mathrm{v}})$ are the dimensionless streamwise and transverse components of the velocity field, $\hat{p}$ is the pressure, $\hat{c}$ is the concentration field, $(u,\ \mathrm{v})$ are the components of the disturbance velocity field, p is the disturbance pressure, c is the disturbance concentration field, and p_s is the basic state pressure.

Substituting (11) into (1)–(3), subtracting the base state, and retaining only terms that are linear in the disturbance amplitude, yields the dimensionless disturbance equations

$$\frac{\partial u}{\partial x} + \frac{\partial \mathrm{v}}{\partial y} = 0, \tag{12a}$$

$$\frac{\partial u}{\partial t} + f'\frac{\partial u}{\partial x} + f''\mathrm{v} = -\frac{\partial p}{\partial x} + \frac{1}{R}\left(v_s\left(\frac{\partial^2 u}{\partial x^2} + \frac{\partial^2 u}{\partial y^2}\right) + v_s'\left(\frac{\partial u}{\partial y} + \frac{\partial \mathrm{v}}{\partial x}\right) + f''\frac{\partial v}{\partial y} + f'''v\right), \tag{12b}$$

$$\frac{\partial \mathrm{v}}{\partial t} + f'\frac{\partial \mathrm{v}}{\partial x} = -\frac{\partial p}{\partial y} + \frac{1}{R}\left(v_s\left(\frac{\partial^2 \mathrm{v}}{\partial y^2} + \frac{\partial^2 \mathrm{v}}{\partial x^2}\right) + 2v_s'\frac{\partial \mathrm{v}}{\partial y} + f''\frac{\partial v}{\partial x}\right), \tag{12c}$$

$$\frac{\partial c}{\partial t} + f'\frac{\partial c}{\partial x} + g'\mathrm{v} = \frac{1}{RSc}\left[\frac{\partial^2 c}{\partial x^2} + \frac{\partial^2 c}{\partial y^2}\right], \tag{12d}$$

where, based on (3), the disturbance to the viscosity is $v = 2ac_sc$. The Reynolds number is defined as $R = (U_1\delta/v_0)$.

The boundary conditions on the disturbances to the velocity and concentration fields are

$$\eta \to \infty, \qquad (u,\ \mathrm{v},\ c) \to (0,\ 0,\ 0), \tag{13a}$$

$$\eta \to -\infty, \qquad (u,\ \mathrm{v},\ c) \to (0,\ 0,\ 0). \tag{13b}$$

We analyze the temporal stability of parallel flow and restrict the analysis to disturbances that are localized in x. The spatial dependence of each disturbance can be separated, if the disturbance is written in the Fourier form as

$$\begin{bmatrix} u \\ \mathrm{v} \\ p \\ c \end{bmatrix}(x,y,t) = \begin{bmatrix} U(y) \\ V(y) \\ P(y) \\ \kappa(y) \end{bmatrix}\exp(\mathrm{i}\alpha x + \beta t), \tag{14}$$

where α is the dimensionless wave number of the disturbance (which can be positive or zero), β is the dimensionless temporal eigenvalue (which can be complex), $P(y)$ is the amplitude of the disturbance to the pressure, $\kappa(y)$ is the amplitude of the disturbance to the concentration, and $U(y)$ and $V(y)$ are the amplitudes of the disturbances to the streamwise and transverse components of the velocity, respectively.

Equation (12a) is satisfied by introducing a disturbance stream function, ψ, such that $u = \partial\psi/\partial y$ and $\mathrm{v} = -\partial\psi/\partial x$. In view of equation (14), $\psi = \varphi(y)\exp(\mathrm{i}\alpha x + \beta t)$ where φ is the amplitude of the disturbance to the stream function. From the relations between the velocity components and stream function we write the amplitudes of the disturbances to the velocity as $U(y) = \varphi'(y)$ and $V(y) = -\mathrm{i}\alpha\varphi(y)$.

Substituting (14) into (12), eliminating pressure, and using the stream function representation for the velocity, yields

$$\alpha R\left[\left(f' - \frac{\mathrm{i}\beta}{\alpha}\right)(\mathrm{i}\alpha^2\varphi - \mathrm{i}\varphi'') + \mathrm{i}f'''\varphi\right] = \left[(1+ag^2)(\varphi''' - \alpha^2\varphi') + 2agg'(\varphi'' + \alpha^2\varphi) + 2a(gf''\kappa)'\right]'$$
$$-\alpha^2[(1+ag^2)(\varphi'' - \alpha^2\varphi) + 4agg'\varphi' - 2af''g\kappa] = 0, \tag{15a}$$

$$\beta\kappa + f\mathrm{i}\alpha\kappa - \mathrm{i}\alpha g'\varphi + \frac{1}{RSc}[\alpha^2\kappa - \kappa''] = 0. \tag{15b}$$

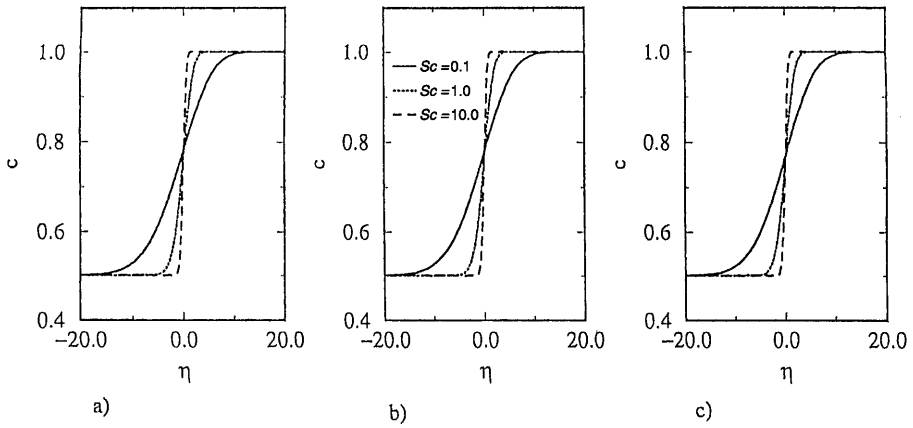

Figure 2. Basic state concentration profiles computed for $U^* = 0.5$, $C^* = 0.5$, and values of Schmidt number $Sc = 0.1, 1.0, 10.0$. Results are presented for (a) $a = 0.1$, (b) $a = 1.0$, and (c) $a = 10.0$.

The associated boundary conditions are

$$\varphi(+\infty) = \varphi'(+\infty) = \kappa(+\infty) = 0 \tag{16a}$$

and

$$\varphi(-\infty) = \varphi'(-\infty) = \kappa(-\infty) = 0. \tag{16b}$$

Equations (15) and (16) describe an eigenvalue problem for the growth rate β and the eigenfunctions $\kappa(y)$ and $\varphi(y)$ as functions of the wave number, α, and the dimensionless parameters ($R,\ Sc,\ a,\ L$). This eigenvalue problem is solved by using the Galerkin technique described in detail in the previous section. A similar set of stability equations has been reported by Pinarbasi and Liakopoulos (1995) in their analysis of the effects of variable viscosity on two-layer Poiseuille flow.

The Galerkin/Chebyshev procedure reduces the stability equations and boundary conditions to generalized matrix eigenvalue problem of the form

$$(\boldsymbol{A} + \beta \boldsymbol{B})\boldsymbol{x} = 0, \tag{17}$$

where $x \in \Re^{2(N+1)}$ are the components of the discretized eigenvectors. The elements of the square matrices $\boldsymbol{A}$ and $\boldsymbol{B}$ in (17), each in $\Re^{2(N+1)x2(N+1)}$, depend on the set of parameters ($\alpha,\ R,\ Sc,\ a,\ L$). The solution of the algebraic eigenanalysis problem (17) is computed using the algorithm DGVCCG available in the IMSL library. The detailed description of the numerical method can be found in Öztekin *et al.* (1997).

For given Sc, L and a the stability of the boundary-free shear flow is expressed by neutral stability curves $R = R(\alpha)$ for which Real(β) = 0. These curves are determined by computing the growth rate β for fixed values of ($\alpha,\ Sc,\ L,\ a$) at several values of Reynolds number R and consequently using bisection to determine the critical value of $R_{cr}(\alpha)$ as Real(β) approaches zero. These searches are carried out to one part in 10^5.

3. Results and Discussions

Stability calculations are presented for various values of Schmidt number Sc and the viscosity parameter a. Calculations are reported for the basic state, followed by calculations for the stability characteristics of the base flow.

The effects of a diffusion layer and viscosity variation on the basic state were explored for a Schmidt number in the range of $0.1 < Sc < 10.0$, and the viscosity parameter, a, of $0.1 < a < 10.0$.

The basic state velocity and concentration profiles are presented for domain size $L = 20$. As long as L is large enough to allow the limits of the profiles to approach approximately the specified far-field boundary conditions, the base state profiles do not vary as L is changed. Basic state concentration profiles are shown in Figure 2 for the values of Schmidt number $Sc = 0.1$, 1.0, and 10.0 and for $a = 0.1$, 1.0, and 10.0. Note

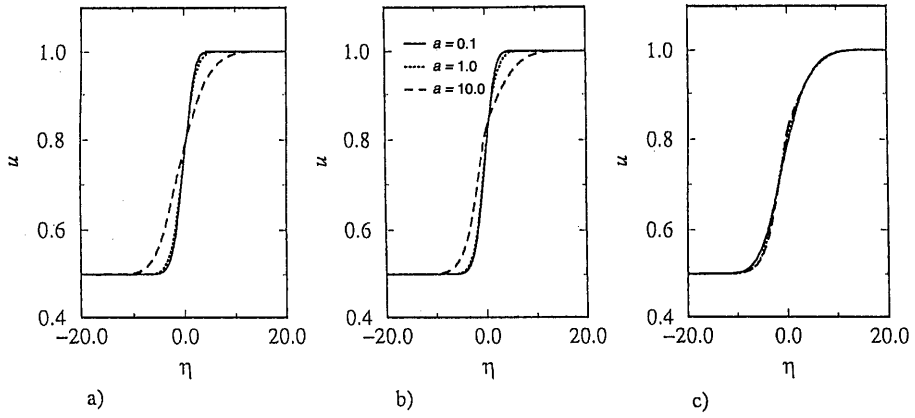

Figure 3. Basic state velocity profiles computed for free shear flows for $U^* = 0.5$, $C^* = 0.5$, and the values of $a = 0.1$, 1.0, and 10.0. Results are presented for (a) $Sc = 0.1$, (b) $Sc = 1.0$, and (c) $Sc = 10.0$.

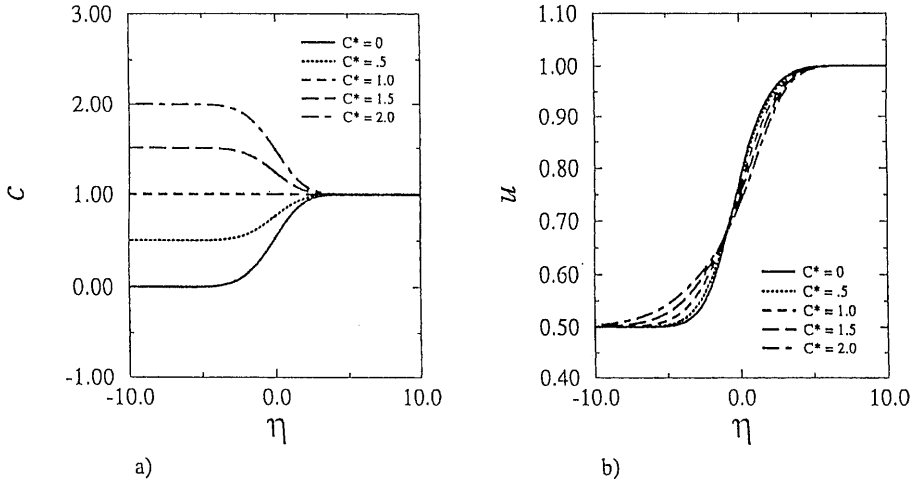

Figure 4. (a) Basic state concentration profiles and (b) velocity profiles for $a = 1.0$, $Sc = 1.0$, $U^* = 0.5$, and various values of the ratio of far-field concentrations, C^*.

that for a fixed value of Sc there is little variation in the concentration profile with varying a. We also note that as the value of Sc increases, the concentration profile becomes accordingly steeper, approaching a sharp interface.

The base state velocity profile $u = u(\eta)$, computed for various values of Sc and a, is shown in Figure 3. The velocity profiles change little with Schmidt number for low values of a, while the velocity profile varies significantly for larger values of a. As Sc is increased to 10.0, however, the effects of a almost vanish, and the u velocity profiles are very similar for all values of a. This indicates that as Sc is increased a limiting base state condition may be approached. The effects of these parameters on the stability of the flow will be explored later. It should be noted that these profiles are computed for $U^* = 0.5$ and $C^* = 0.5$. These parameters are used throughout, unless otherwise stated.

The effect of varying C^* and U^* on the basic state velocity and concentration profiles are illustrated in Figures 4 and 5 for $Sc = 1.0$ and $a = 1.0$. We note that for $C^* > 1$ the u velocity profile changes more gradually and approaches the free stream velocity more slowly in the region $\eta < 0$. For $C^* < 1$ the velocity profile changes more abruptly than for the case of zero concentration gradient ($C^* = 1.0$), as shown in Figure 5. This can be explained by the fact that in the case of $C^* > 1$ the diffusion slows the momentum change in the region $\eta < 0$, due to the relation of viscosity with concentration. When the direction of the diffusion is reversed ($C^* < 1$), the momentum change is increased in the $\eta < 0$ region due to the lower level of concentration. We also note that the concentration profile changes more gradually for $\eta < 0$ as

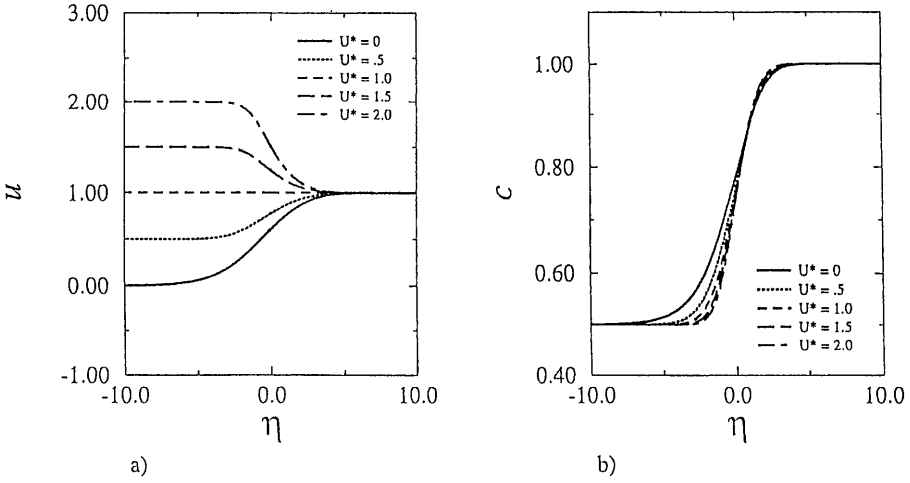

Figure 5. (a) Basic state velocity profiles and (b) concentration profiles for a = 1.0, Sc = 1.0, C^* = 0.5, and various values of the ratio of far-field velocities, U^*.

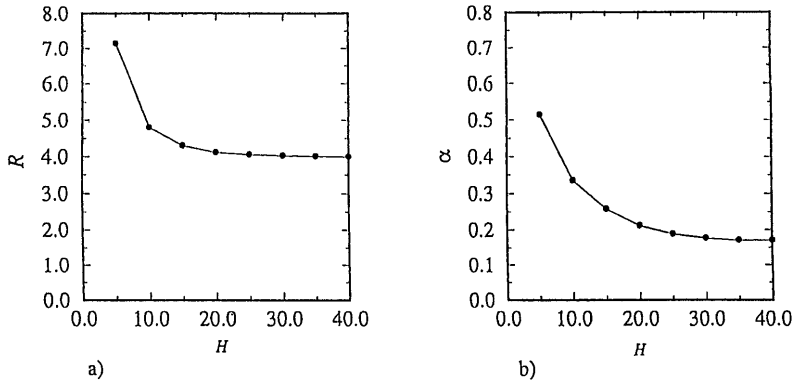

Figure 6. Stability boundaries (a) $R_{\rm cr} = R_{\rm cr}(H)$ and (b) $\alpha_{\rm cr} = \alpha_{\rm cr}(H)$ computed for jet flow with base velocity profile $u = \text{sech}^2(y)$.

U^* is increased. This is due to the fact that the increased flow velocity in the $\eta < 0$ region slows the rate of diffusion. These results clearly show that the coupling between the base state momentum and diffusion equations is properly occurring. The effect of these trends on the stability of the flow will be discussed later.

The stability code was first tested by calculating the stability of laminar jet flow of the form $u = U\ \text{sech}^2(y/H)$, where H denotes the half-width of the jet and U is the centerline velocity. We first compute the neutral stability curves $R = R(\alpha)$ for a fixed value of domain size L (L is equivalent to H), and then determine the critical value of Reynolds number, $R_{\rm cr}$, for each domain size L. Note that corresponds to the minimum in the neutral stability curve $R = R(\alpha)$. For $R > R_{\rm cr}(\alpha_{\rm cr})$ the flow is unstable to disturbances in some range of the wave number α, while for $R < R_{\rm cr}(\alpha_{\rm cr})$ the flow is stable for all values of α.

The critical Reynolds number $R_{\rm cr}$ and the wave number $\alpha_{\rm cr}$ are plotted in Figure 6 versus the domain size L. The critical Reynolds number decreases monotonically as L increases and asymptotically approaches $R_{\rm cr}$ = 4. Similarly, the critical wave number asymptotes to 0.17 as L increases. The critical parameters predicted here for free jet flows are in good agreement with the stability results of Tatsumi and Kakutani (1958). This ensures that the numerical code employed to solve the disturbance equations predicts stability results that are consistent with previous stability studies of laminar jet flow.

The accuracy of the Galerkin/Chebyshev approximation for the eigenvalue problem (17) was tested by checking the spectral convergence of the most unstable eigenvalue (the eigenvalue with the smallest real part). The real part of the least stable eigenvalue is plotted in Figure 7 as a function of the number of Chebyshev polynomials N in the expansions for parameter values of α, L, R and for a = 1.0, Sc = 1.0,

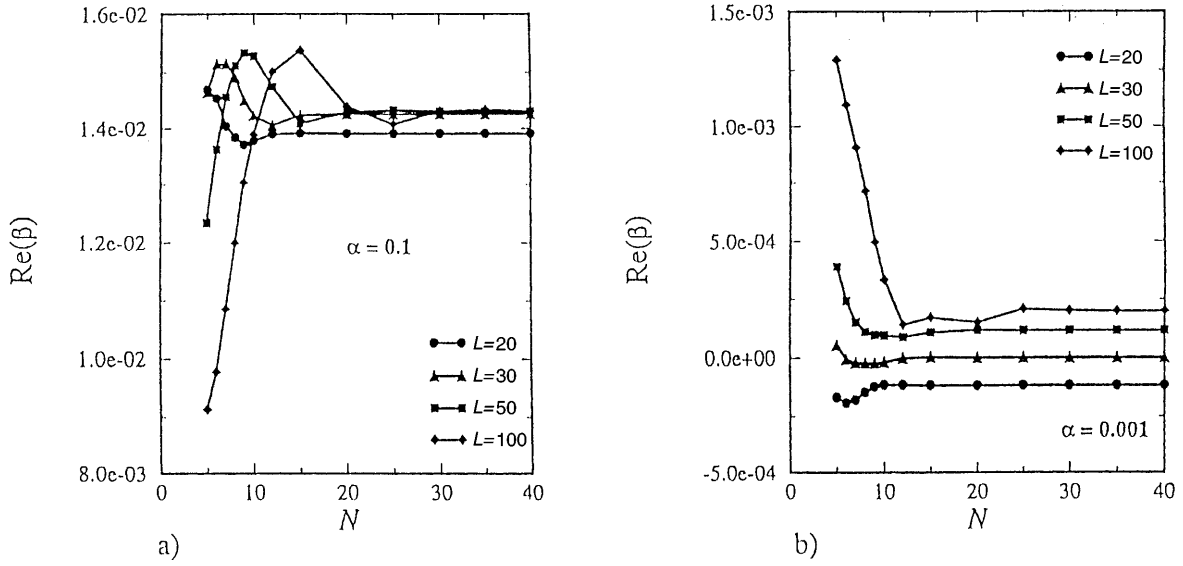

Figure 7. Real part of the least stable eigenvalue β, Re(β), versus N computed for R = 100, a = 1.0, Sc = 1.0, U^* = 0.5, C^* = 0.5, and computational domain sizes of L = 20, 30, 50, and 100. Results are presented for (a) α = 0.1 and (b) α = 0.001.

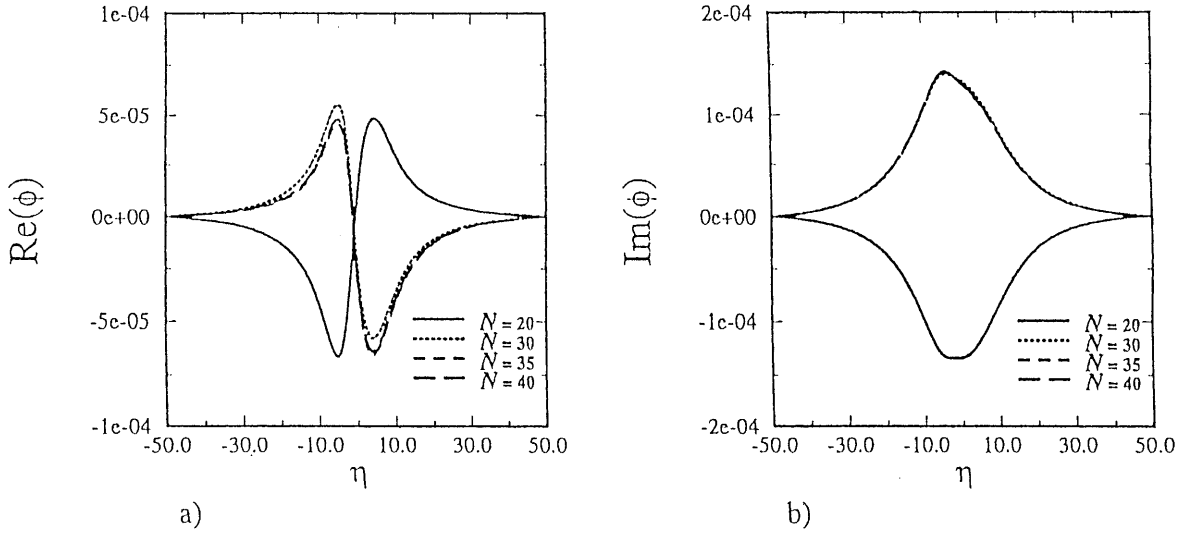

Figure 8. The profiles of (a) the real (solid curves) and (b) imaginary (dashed curve) parts of the disturbance stream function, $\varphi(y)$ for $20 \leq N \leq 40$, with R = 10.0, Sc = 1.0, α = 0.1, a = 1.0, C^* = 0.5, and U^* = 0.5. N is the number of the Chebyshev polynomials.

U^* = 0.5, and C^* = 0.5. For R = 100 and different values of computational domain size L, Figure 7 shows the real part of the least stable eigenvalue, Re(β) plotted versus N. As shown in Figure 7 for R = 100, the Re(β) converges to one part in 10^3 for all L for N of about 15 and 20 for α = 0.1 and α = 0.001, respectively. Similar spectral convergence is observed for different values of system parameters. We use $N \geq 30$ in the stability calculations to compute the neutral stability curves and diagrams presented below.

The profiles of the real and imaginary parts of the disturbance stream function, $\varphi(\eta)$, computed for R = 10.0, Sc = 1.0, α = 0.1, a = 1.0, C^* = 0.5, and U^* = 0.5 are shown in Figure 8. For computational domain size L = 50 the disturbance stream function is plotted for N = 20, 30, 35, and 40. Both the real, Re(φ), and imaginary, Im(φ), parts of the disturbance stream function converge as N is increased.

The growth rate (the real part of the least stable eigenvalue) Re(β) is shown in Figure 9 as a function of wave number, α, for different values of Reynolds number with L = 100. Note that the value of Re(β)

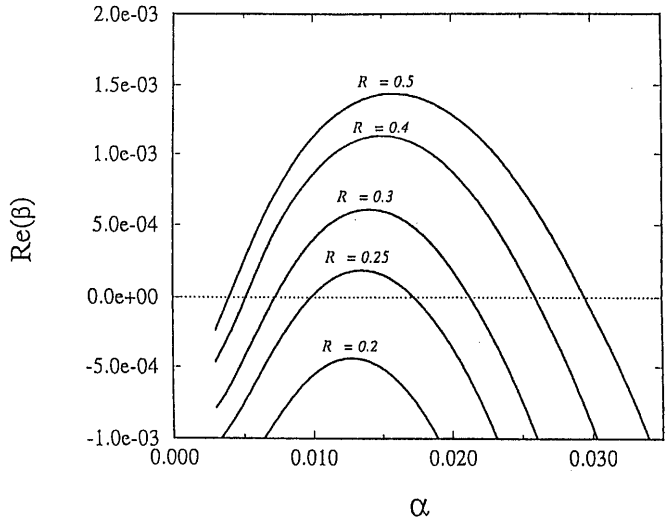

Figure 9. Growth rate, Re(β) versus wave number, α, for L = 100, a = 1.0, Sc = 1.0, U^* = 0.5, C^* = 0.5, and 0.2 $\leq$ Re $\leq$ 0.5.

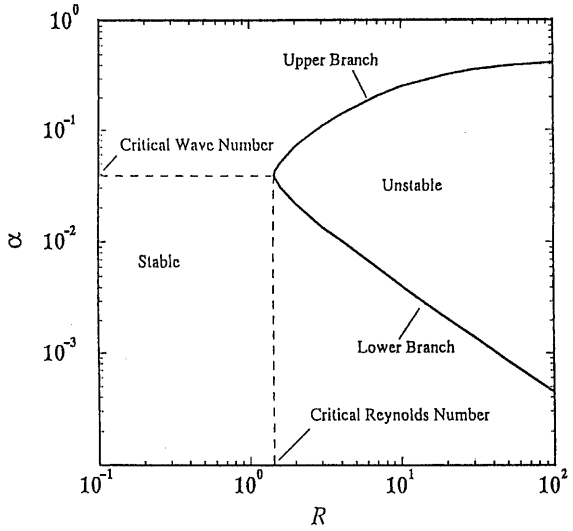

Figure 10. Neutral stability curve $R = R(\alpha)$ illustrating stable and unstable regions, critical wave number, critical Reynolds number, and lower and upper branch. Plotted for L = 50, a = 0, U^* = 0.5, and C^* = 0.5.

increases at all values of α, as R is increased. Therefore, the flow becomes less stable with increasing R, as is expected.

The neutral stability curve $R = R(\alpha)$ is formed from the computation of growth rates for various values of L. These curves determine the stable and unstable regions in the (R, α) plane. At a fixed R, the values of wave number on the neutral curve are found for which Re(β) = 0. For the family of the flows examined in this work, two values of α satisfying Re(β) = 0 are found for each R above the critical Reynolds number. These points are plotted for a number of different R and formed into curves. The curve formed by the lower values of α is known as the lower branch, and, likewise, the larger α curve is the upper branch. The location where these curves meet determines the minimum point for the entire neutral curve and yields the critical Reynolds number $R_{\rm cr}$. Likewise, the corresponding value of α at this minimum is referred to as $\alpha_{\rm cr}$. We first choose the case with constant viscosity (a = 0) and create neutral curves (R versus α) for different values of L. Figure 10 illustrates the plot of the neutral curve for L = 50. Here, the stable and unstable regions are labeled, as well as $R_{\rm cr}$, $\alpha_{\rm cr}$, and the lower and upper branches.

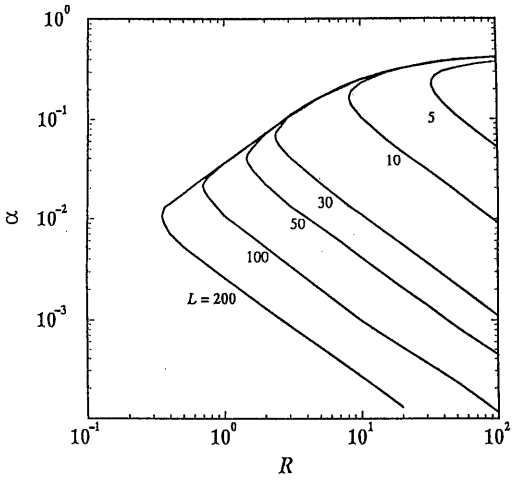

Figure 11. Neutral stability curves $R = R(\alpha)$ for computational domain sizes, $5 \leq L \leq 200$. Plotted for $a = 0$, $U^* = 0.5$, and $C^* = 0.5$.

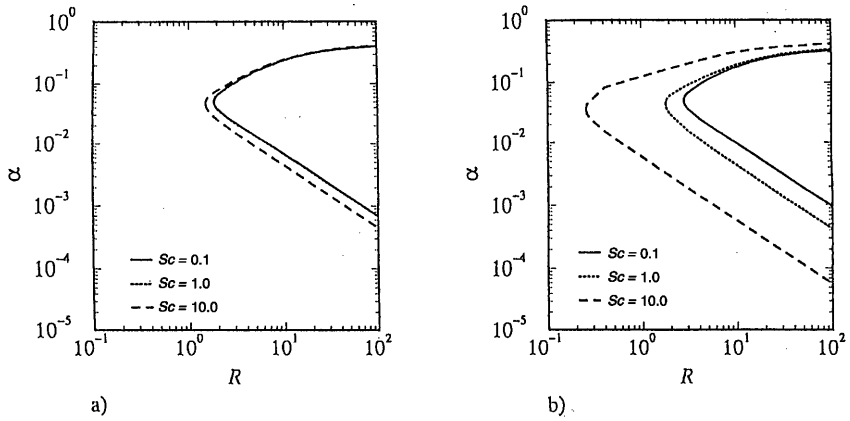

Figure 12. Neutral stability curves $R = R(\alpha)$ computed for $U^* = 0.5$, $C^* = 0.5$ and various values of Schmidt number, $Sc = 0.1$, 1.0, and 10.0. Results shown for (a) $a = 0.1$ and (b) $a = 1.0$.

As the value of L increases, the lower branch of the neutral curve shifts downward (the unstable region in R–α plane becomes larger), or rather the values of α for Re(β) = 0 are smaller for corresponding R (see Figure 11). The limit of α for stability at a given Reynolds number varies inversely with L. This trend strongly suggests that a nonzero Reynolds number where the flow will be stable for all values of α does not exist, and that the flow must be unstable for all R. Similar results are obtained for the variable viscosity case $a \neq 0$ as well.

In order to investigate the effects of diffusion and viscosity stratification on the temporal stability of the parallel shear flow, the neutral stability curves are calculated for various values of Sc and a. These results are summarized in Figure 12 where the neutral stability curves $R = R(\alpha)$ for a of 0.1 and 1.0 and for Sc = 0.1, 1.0, and 10.0, with L = 40, are presented. For a = 0.1 there is almost no difference between the neutral stability curves predicted for Sc = 0.1 and 1.0, as shown in Figure 12(a). As the Schmidt number is increased to 10.0, it is apparent that the flow becomes less stable and $R_{\rm cr}$ decreases to about 1.6. It should be noted, however, that for a relatively small value of a the limit to which the upper neutral curve converges to as L grows, changes very little with Sc, as might be expected. For larger values of a the effects of Sc are more pronounced on both lower and upper branches of the neutral curve. As Sc increases the unstable region in the R–α plane becomes larger and the critical Reynolds number becomes smaller. Note that for small values of α (lower branch) the diffusion and viscosity stratification destabilize the flow whereas for larger α (upper branch) these effects diminish as Reynolds number increases.

4. Conclusions

A linear stability analysis of boundary-free shear flows has been presented. The effect of diffusion and viscosity stratification due to the concentration gradient on the stability characteristics of the shear flow has been investigated. It has been found that the base shear flow is destabilized with increasing value of Sc, indicating that species diffusion has a destabilizing influence on the boundary-free shear flow. It has also been shown that viscosity stratification due to the presence of a concentration gradient has a destabilizing effect on the shear flow. These destabilizing effects of diffusion and viscosity stratification are stronger on the lower branches of the neutral stability curves than on the upper branches (see Figure 12).

The critical Reynolds number above which shear flow becomes unstable, R_{cr}, remains zero despite the presence of transport of species and the viscosity variation due to the concentration gradient. This trend is consistent with the fact that the flow appears to be destabilized with increasing effects of a concentration gradient and the viscosity stratification, or more explicitly, increasing Sc and viscosity parameter a. Therefore, it would not be expected that the effects of concentration would give way to the flow having a nonzero critical Reynolds number. From a physical point of view, these results can be explained by the fact that the transport of species through the shear layer may serve as an additional disturbance-causing mechanism, where diffusion must excite rather than dampen infinitesimal disturbances.

Another aspect of the problem that may have to be explored is the assumption of parallel flow in the stability analysis. Due to the fact that we are concerned with low R boundary-free flows, the assumption that $v(y)$ is much less than $u(y)$ may be invalid. Although, the inclusion of the y-direction base velocity component in the stability analysis will considerably complicate the problem, it may prove necessary in accurately predicting the stability characteristics of the flow. A nonzero critical value of R is expected when nonparallel effects in the base flow are included.

Since the mean velocity profile is slowly varying in the streamwise direction, the first order corrections to the parallel stability analysis can be made by a multiple scale expansion in terms of a suitable small parameter defining the slow variation of the mean flow (Crighton and Gaster, 1976; Gaster *et al.*, 1985; Nayfeh and El-Hady, 1980; Asrar and Nayfeh, 1985). This method essentially reformulates the problem as a stability analysis of a "locally parallel flow" and generates a correction to the parallel flow stability calculations. The amplitude of the disturbances varies in the streamwise direction and satisfies an appropriate amplitude equation (see details in Crighton and Gaster (1976)). The disturbances, in fact, can peak at some downstream locations. These flow features have been observed in early experiments in jets and other free shear flows (Crow and Champagne, 1971; Moore, 1977), but they cannot be predicted by parallel flow stability analysis. The nonparallel contributions could be more significant when the fluid properties are dependent on temperature or concentration as is the case in the present work. These effects are currently being examined.

References

Asrar, W., and Nayfeh, A.H. (1985) Nonparallel stability of heated two-dimensional boundary layers. *Phys. Fluids* **28**, 1263–1272.

Azaiez, J., and Homsy, G.M. (1993) Linear stability of free shear flow of viscoelastic liquids. *J. Fluid Mech.* **268**, 37–69.

Betchov, R., and Criminale, W.O. (1967) *Stability of Parallel Flows*. Academic Press, New York.

Betchov, R., and Szewczyk, A. (1963) Stability of a shear layer between parallel streams. *Phys. Fluids* **6**(10), 1391–1396.

Bird, R.B, Armstrong, R.C., and Hassager, O. (1987a) *Dynamics of Polymeric Liquids*, Volume 1, 2nd edition. Wiley Interscience, New York.

Bird, R.B., Curtiss, C.F., Armstrong, R.C., and Hassager, O. (1987b) *Dynamics of Polymeric Liquids*, Volume 2, 2nd edition. Wiley Interscience, New York.

Corcos, G.M., and Lin, S. (1984) The mixing layer: deterministic models of a turbulent flow. *J. Fluid Mech.* **139**, 67–95.

Crighton, D.G., and Gaster, M. (1976) Stability of slowly diverging jet flow. *J. Fluid Mech.* **77**, 397–413.

Crow, S.C., and Champagne, F.H. (1971) Orderly structure in jet turbulence. *J. Fluid Mech.* **48**, 547–591.

Drazin, P.G., and Howard, L.N. (1962) The instability to long waves of unbounded parallel inviscid flow. *J. Fluid. Mech.* **14**, 257–283.

Drazin, P.G., and Reid, W.H. (1981) *Hydrodynamic Stability*. Cambridge University Press, Cambridge.

Esch, R.E. (1957) The instability of a shear layer between two parallel streams. *J. Fluid. Mech.* **3**, 289–303.

Gaster, M., Kit, E., and Wygnanski, I. (1985) Large-scale structures in a forced turbulent mixing layer. *J. Fluid Mech.* **150**, 23–39.

Grosch, C.E., and Jackson, T.L. (1991) Inviscid spatial stability of a three-dimensional compressible mixing layer. *J. Fluid Mech.* **231**, 35–40.

Helmholtz, H. (1868) Discontinuous fluid motions. *Monatl. Konigl. Preuss. Akad. Wiss. Berlin* **23**, 215–288.

Ho, C., and Huerre, P. (1984) Perturbed free shear layers. *Ann. Rev. Fluid Mech.* **16**, 365–424.
Incropera, F.P., and DeWitt, D.P. (1990) Fundamentals of Heat and Mass Transfer. Wiley, New York.
Jackson, T.L., and Grosch, C.E. (1989) Inviscid spatial stability of a compressible mixing layer. *J. Fluid Mech*. **208**, 609–637.
Jackson, T.L., and Grosch, C.E. (1990a) Inviscid spatial stability of a compressible mixing layer. Part 2. The flame sheet model. *J. Fluid Mech*. **217**, 391–420.
Jackson, T.L., and Grosch, C.E. (1990b) Absolute/convective instabilities and the convective Mach number in a compressible mixing layer. *Phys. Fluids A* **6**, 949.
Jackson, T.L., and Grosch, C.E. (1991) Inviscid spatial stability of a compressible mixing layer. Part 3. Effect of thermodynamics. *J. Fluid Mech*. **224**, 159–175.
Jackson, T.L., and Grosch, C.E. (1994) Structure and stability of a laminar diffusion flame in a compressible, three-dimensional mixing layer. *Theoret. Comput. Fluid Dynamics* **6**, 89–112.
Kennedy, C.A., and Gatski, T.B. (1994) Self-similar supersonic variable-density shear layers in binary systems. *Phys. Fluids* **6**(2), 662–673.
Kelvin, L. (1871) Hydrokinetic solutions and observations. *Philos. Mag*. **42**(4), 362–377.
Kozusko, F., Grosch, C.E., Jackson, T.L., Kennedy, C.A., and Gatski, T.B. (1996a) The structure of variable property, compressible mixing layers in binary mixtures. *Phys. Fluids* **8**(7), 1945–1953.
Kozusko, F., Lasseigne, D.G., Grosch, C.E., and Jackson, T.L. (1996b) The stability of compressible mixing layers in binary gases. *Phys. Fluids* **8**(7), 1954–1963.
Lessen, M. (1950) *Rep. Nat. Adv. Comm. Aero., Wash. No*. 979.
Liu, J.T.C. (1974) Developing large scale wavelike eddies and the near jet noise field. *J. Fluid Mech*. **62**, 437–464.
Maitland, G.C., Rigby, M., Smith, E.B., and Wakeham, W.A. (1981) Intermolecular Forces (Their Origin and Determination). Clarendon Press, Oxford.
Metcalfe, R.W., Orzag, S.A., Brachet, M.E., Menon, S., and Riley, J.J. (1987) Secondary instability of a temporally growing mixing layer. *J. Fluid Mech*. **184**, 207–243.
Michalke, A. (1964) On the inviscid instability of the hyperbolic-tangent velocity profile. *J. Fluid Mech*. **19**, 543–556.
Moore, C.J. (1977) The role of shear layer instability waves in jet exhaust noise. *J. Fluid Mech*. **80**, 321–367.
Morris, P. (1971) The structure of turbulent shear flow. Ph.D. thesis, Southampton University.
Nayfeh, A.H., and El-Hady, N.M. (1980) Nonparallel stability of two-dimensional nonuniformly heated boundary-layer layers. *Phys. Fluids* **23**, 10–18.
Öztekin, A., Alakus, B., and McKinley, G.H. (1997) Stability of planar stagnation flow of highly viscoelastic fluid, *J. Non-Newtonian Fluid Mech.* **72**, 1–29.
Panton, R.L. (1984) *Incompressible Flow*. Wiley, New York.
Pinarbasi, A., and Liakopoulos A. (1995) The effect of variable viscosity on the interfacial stability of two-layer Pouiseuille flow. *Phys. Fluids*. **7**(6), 1318–1324.
Rogers, M.M., and Moser, R.D. (1992) The three-dimensional evolution of a plane mixing layer: the Kelvin-Helmholtz roll-up. *J. Fluid. Mech*. **243**, 183–226.
Schlichting, H. (1979) *Boundary Layer Theory*. McGraw-Hill, New York.
Shin, D.S., and Ferziger, J.H. (1993) Linear stability of the confined compressible reacting mixing layer. *AIAA J*. **31**, 571–577.
Shoemaker, D.P., Garland, C.G., and Steinfeld, J.I. (1974) *Experiments in Physical Chemistry*, 3rd edition. McGraw-Hill, New York.
Strazisar, A.J., and Reshotko, E. (1978) Stability of heated laminar boundary layers in water with nonuniform surface temperature. *Phys. Fluids* **21**, 727–735.
Sullivan, G.D., and List, E.J. (1994) On mixing and transport at a sheared density interface. *J. Fluid Mech*. **273**, 213–239.
Tatsumi, T., and Gotoh, K. (1959) The stability of free boundary layers between two uniform streams. *J. Fluid Mech*. **7**, 433–441.
Tatsumi, T., and Kakutani, T. (1958) The stability of a two-dimensional laminar jet. *J. Fluid Mech*. **4**, 261–275.
Zebib, A. (1987) Removal of spurious modes encountered in solving stability problems by spectral methods. *J. Comput. Phys*. **70**, 521–525.